Journal of Systems Engineering and Electronics
Vol. 32, No. 3, June 2021, pp.517 – 526

Integrating electromagnetic surface and antenna array for reflection suppression and excellent radiation

ZHENG Yuejun*, DING Liang, CHEN Qiang, GUO Min, and FU Yunqi
College of Electronic Science and Technology, National University of Defense Technology, Changsha 410073, China

Abstract: The electromagnetic surface antenna array (EMSAA) has been proposed for obtaining reflection suppression and excellent radiation simultaneously. The antenna with rectangular radiation patch is used to design anisotropic electromagnetic surface. Preternatural reflection characteristics of the element antenna can be tailored depending on the incident polarizations. EMSAA can be constructed by using single structured element antenna with 90° rotation and orthometric arrangement. This orthometric arrangement of EMSAA is helpful to achieve reflection suppression and excellent radiation. The simulated results show that the reflection of EMSAA is suppressed from 5.0 GHz to 8.0 GHz with peak reduction of 12.3 dB. The linear- and circular-polarized radiation properties of EMSAA are obtained and the maximum gain is 14.3 dBi. The measured results are consistent with the simulation results. The results demonstrate that the reflection suppression and excellent radiation are achieved simultaneously. Such design of EMSAA will open the path for integrating antenna fields and electromagnetic surface (EMS) fields.

Keywords: electromagnetic surface (EMS), antenna array, radiation, reflection.

DOI: 10.23919/JSEE.2021.000043

1. Introduction

Electromagnetic surfaces (EMSs) are two-dimensional planar artificial surfaces with rationally designed shapes, sizes, and compositions. The EMSs provide exceptional capabilities for manipulating the magnitudes, phases, polarizations of electromagnetic waves [1−4]. Thus, the EMSs attract focus investigations and extensive applications [5−8], such as reflection suppression [7,8]. Recently, various techniques have been reported to suppress reflection by utilizing the EMSs [9−17], among which a representative method was constructing artificial magnetic surface by combining the surface structure with perfect electric surface in a chessboard configuration [9]. This method takes advantage of the reflection and provides flexibility to suppress reflection. Subsequently, more and more excellent works were reported to obtain wideband reflection suppression [10−15] or multifunctional performance [16,17].

As a promising application, this kind of reflective EMS is applied to suppress reflection of a single antenna [18−20] or an antenna array [21−26]. This method is useful for the single antenna. Although the reflection of the antenna array is suppressed by utilizing this method, challenges still exist. For example, the design of the EMS and the antenna array is divided. The effect on radiation and reflection suppression is uncertain. Moreover, the vacant area of the antenna array is limited. The characteristics of EMS is influenced because of the restricted units. As a result, the performance of the antenna array is influenced. The radiation and the reflection suppression of the antenna array are difficult to control simultaneously.

To overcome the above challenges, the concept of EMS is introduced into antenna design. The antenna with rectangular radiation patch is utilized to form anisotropic EMS. The antenna has preternatural reflection characteristics and good radiation properties simultaneously. Two different antenna elements are used to form the antenna array [27,28]. Good radiation properties and reflection suppression are obtained simultaneously. This is a novel way to design antennas and overcome the challenges. In the above designs, two different antenna elements are utilized. However, in some applications only one kind of antenna element can be used, and multiple polarizations are required. Based on the excellent works, the anisotropic structures of antenna array are utilized [29]. As a result, the circular-polarized radiation and reflection suppression properties are obtained, respectively. However, the radiation area is reduced and the gain is influenced by using the split ring resonators. Moreover, the reflection is

Manuscript received September 15, 2020.
*Corresponding author.
This work was supported by the National Natural Science Foundation of China (61901493; 61901492), the Natural Science Foundation of Hunan Province (2020JJ5676), and the Science and Technology Innovation Program of Hunan Province (2020RC2048).

suppressed when the feeding of the antenna array is open-circuited. The radiation and reflection suppression of the antenna array cannot be realized simultaneously. To enhance the gain, a novel loading method and varactors are used [30].

In this paper, the rectangular radiation patch of the element antenna is utilized, which is beneficial to construct an anisotropic EMS. The electromagnetic surface antenna array (EMSAA) is formed by using single structured element antenna with 90° rotation and orthometric arrangement [7,29]. This orthometric arrangement of EMSAA is helpful to achieve reflection suppression and excellent radiation. For using rectangular radiation patch, the gain of EMSAA is maintained. Meanwhile, the linear- and circular-polarized radiation properties are achieved. Moreover, the reflection is suppressed when the feeding of the antenna array is well matched. Thus, the reflection suppression and excellent radiation of EMSAA are achieved simultaneously.

2. Design of EMSAA element

According to the above analysis, the patch antenna with rectangular radiation patch is selected as basic elements to construct EMSAA. As Fig. 1 shows, the designed rectangular radiation patch is etched on the top surface of dielectric substrate. The metallic ground plane is installed on the bottom surface to guarantee absolute reflection. Polytef dielectric slab (F4B) is adopted as the substrate (ε=2.65, tan δ=0.002). The elements of EMSAA are fed with 50 Ω coaxial probes for impedance matching. The optimized design parameters are P=22.4, t=3.0, L=11.8, W=14.8, lf=3.7, units: mm. For easy of description, the element with coaxial probe skewing x-axis is denoted as E1 and the other one is denoted as E2. E2 is obtained by rotating 90° of E1. E1 and E2 own the same structures and parameters, so E1 and E2 are the same element.

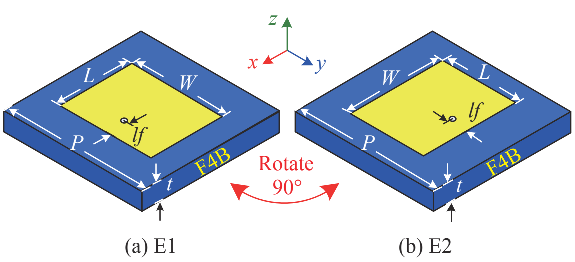

Fig. 1 Schematic geometry of the EMSAA elements

Because the concept of EMS is introduced into antenna design, radiation and reflection properties of the elements are taken into consideration simultaneously. For radiation properties, the basic element is designed based on the empirical formula of patch antenna design. For reflection properties, the basic element is designed based on the phase cancellation principle. According to the array theory, the total scattering electric field can be given as

$$\vec{E}_{\rm sca} = \vec{E}_{\rm r1}AF_1 + \vec{E}_{\rm r2}AF_2 \tag{1}$$

where $\vec{E}_{\rm r1}$ and $\vec{E}_{\rm r2}$ are the reflection electric fields of the elements E1 and E2, and AF_1 and AF_2 are the array factors. The reflection electric field $\vec{E}_{\rm r1}$ and $\vec{E}_{\rm r2}$ can be expressed as

$$\vec{E}_{\rm r1} = E_{\rm r1}{\rm e}^{{\rm j}\varphi_{\rm r1}}\vec{e}_{\rm r1} \tag{2}$$

$$\vec{E}_{\rm r2} = E_{\rm r2}{\rm e}^{{\rm j}\varphi_{\rm r2}}\vec{e}_{\rm r2} \tag{3}$$

where $E_{\rm r1}$, $\varphi_{\rm r1}$ and $E_{\rm r2}$, $\varphi_{\rm r2}$ are the magnitudes and phases of electric field reflected by E1 and E2, respectively. For the scattering electric field $\vec{E}_{\rm sca}$, the reflection suppression is produced when the phase difference satisfies the following condition [11,14]:

$$150^\circ \leqslant |\varphi_{\rm r1}-\varphi_{\rm r2}| \leqslant 210^\circ. \tag{4}$$

In this design, the phase difference condition of the asymmetric element can be represented as

$$150^\circ \leqslant |\varphi_{{\rm r}x}-\varphi_{{\rm r}y}| \leqslant 210^\circ \tag{5}$$

where $\varphi_{{\rm r}x}$ and $\varphi_{{\rm r}y}$ are the phases of the electric field reflected by the elements for x and y polarized incidence, respectively. From the above analysis, the radiation and reflection properties of the elements could be achieved simultaneously.

For demonstrating the above design mechanism, the element antenna E1 is taken as an example. Full-wave numerical analysis is carried out in the Ansoft HFSS. The radiation boundary condition and lumped port excitation are used to achieve radiation properties. Meanwhile, the master-slave periodic boundary condition and floquet port excitation are utilized to obtain reflection properties. To acquire the desired radiation and reflection properties, all parameters of the element antenna are optimized.

The radiation properties of the element antenna E1 are shown in Fig. 2. The E1 resonates at 6.76 GHz and good impedance matching is achieved. The radiation patterns at 6.76 GHz are depicted in Fig. 2(b). The 2D radiation patterns show that main-beam patterns are all along normal direction and the maximum gain is 7.1 dBi. It can be concluded that the element antenna of EMSAA achieves good radiation properties.

The reflection characteristics of the element antenna E1 are shown in Fig. 3. As Fig. 3(a) plots, the reflection magnitudes are decreased for x-polarized incidence while maintained for y -polarized incidence. The x-polarized waves are partially absorbed from 5.0 GHz to 8.0 GHz. The 0° reflection phases at 6.65 GHz (x-pol) and 5.2 GHz (y-pol) are achieved, respectively. Phase difference between 150° and 210° is obtained from 5.4 GHz to 6.7 GHz, shown in Fig. 3(b). From the above analysis, reflection suppression of EMSAA is expected based on phase cancellation and the absorption principle.

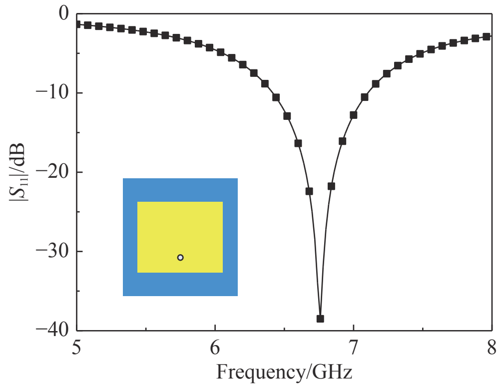

(a) $|S_{11}|$

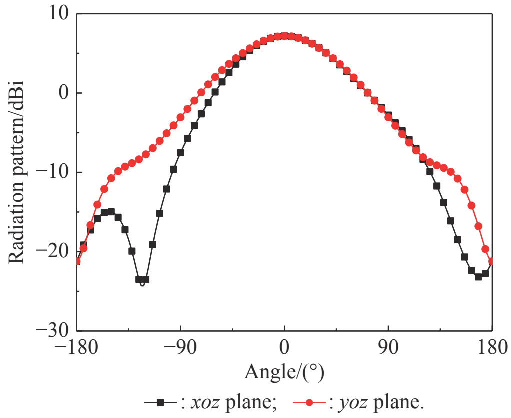

(b) 2D radiation patterns

Fig. 2 Radiation properties of EMSAA element

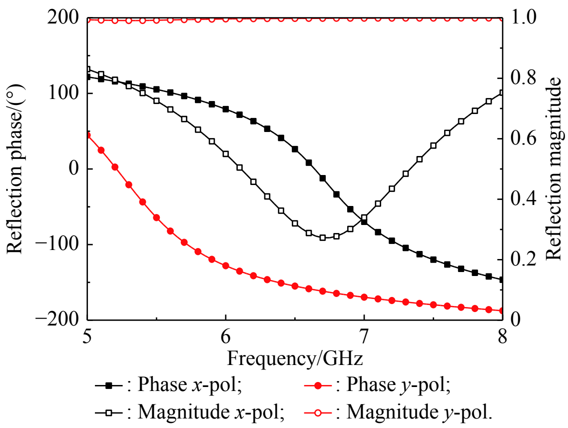

(a) Phases and magnitudes

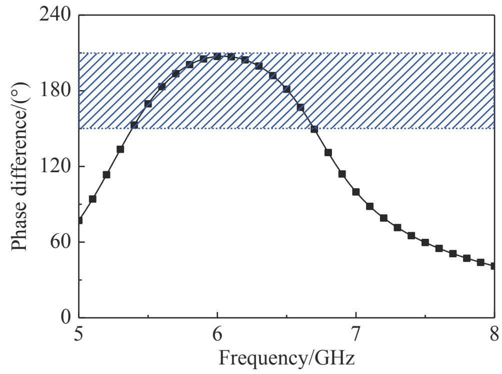

(b) Phase difference

Fig. 3 Reflection properties of EMSAA elements

3. Analysis and performance of EMSAA

As for the asymmetric EMSAA elements, the reflection suppression will be influenced by the arrangement. The grated and orthometric arrangements are studied for obtaining better reflection suppression. The grated and orthometric arrangements shown in Fig. 4(a) and Fig. 4(c) are arranged with a single element while in Fig. 4(b) and Fig. 4(d) are ordered with the element tile. For easy of description, the four arrangements of EMSAA are denoted as EMSAA1, EMSAA2, EMSAA3 and EMSAA4, respectively.

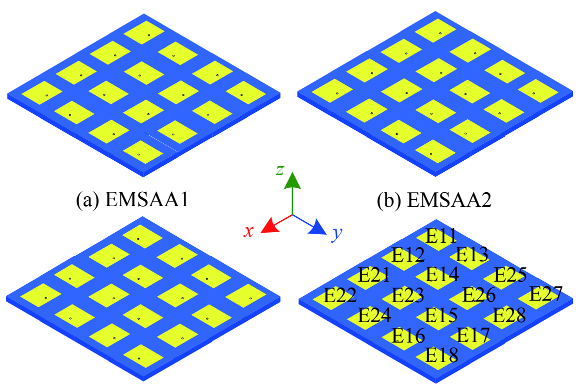

(a) EMSAA1 (b) EMSAA2

(c) EMSAA3 (d) EMSAA4

Fig. 4 Different arrangements of EMSAA

The reflection properties of the four different EMSAAs are investigated and the results are shown in Fig. 5. For the grated arrangements, the reflection suppression of EMSAA2 is better than that of EMSAA1 for x-polarized incidence while the reflection suppression of EMSAA1 is better than that of EMSAA2 for y -polarized incidence. For the orthometric arrangements, the reflection suppression of EMSAA4 is better than that of EMSAA3 for x- and y-polarized incidences. Considering both x- and y-polarized incidences, it can be concluded that better reflection suppressions can be achieved by arranging EMSAA with the element tile. The reflection suppressions of EM-

SAA2 and EMSAA4 are almost the same. Thus, EMSAA2 and EMSAA4 are selected as the candidates. Referring to previous works [7,29], EMSAA4 possesses the ability to radiate circular polarization waves when the four element tiles rotate with a step 90° phase difference one by one along the anticlockwise. In this design, both radiation and scattering properties are taken into consideration. Thus, the orthometric arrangement of EMSAA4 is selected as the final arrangement of EMSAA. For easy description, each element of EMSAA is coded. As Fig. 4(d) shows, the coding order is from $-x$ to $+x$ and from $-y$ to $+y$.

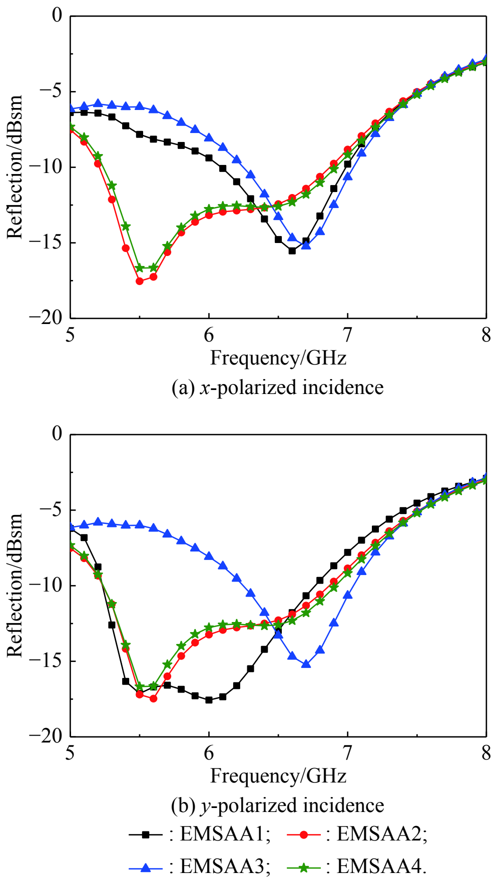

Fig. 5 Reflection properties of EMSAA

Because the EMSAA has a symmetrical structure, the reflection suppression properties of the EMSAA under x-polarized incidence are presented in Fig. 6. Because EMSAA can be treated as the EMS, a same sized metallic plane is taken as a comparison. For normal incidence, remarkable reflection suppression is achieved from 5.0 GHz to 8.0 GHz. The operation band of EMSAA is covered and in-band reflection suppression is obtained. The peak reflection suppression reaches 12.3 dB.

A 3D reflection patterns comparison of the EMSAA and the same size metallic plane is plotted in Fig. 7. For normal incidence, the strong backward scattering is redirected to four quadrants and the scattering power is weakened at 5.55 GHz, shown in Fig. 7(a) and Fig. 7(b). It indicates that reflection suppression at 5.55 GHz is achieved based on the phase cancellation principle and the absorption principle. As Fig. 7(c) and Fig. 7(d) present, planar pattern along normal direction is observed at 6.76 GHz, and the scattering power is also weakened. It infers that reflection suppression at 6.76 GHz is mainly obtained for the absorption of impedance matching. From the above analysis, it can be concluded that the EMSAA owns good reflection suppression properties.

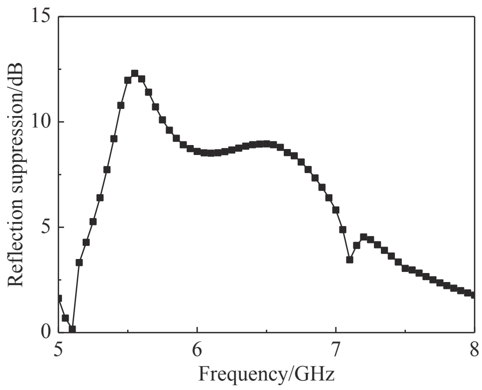

Fig. 6 Reflection suppression of EMSAA for different incident angles

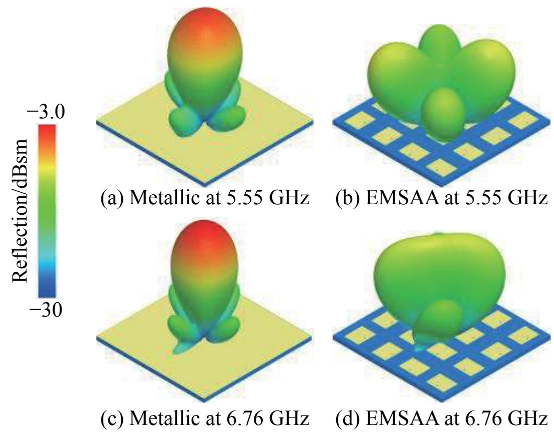

Fig. 7 3D reflection patterns

Since the elements E1 and E2 can be fed independently, the radiation properties are analyzed based on the feeding solution. Firstly, only the E1 elements are fed and the feeding phase is 0°. The radiation properties of EMSAA in this feeding solution are investigated and shown in Fig. 8. To describe reflection coefficients $|S_{11}|$ of EMSAA, the diagonal elements of EMSAA are selected (E11, E14, E15, E18). As Fig. 8(a) presents, the elements resonate close to 6.76 GHz and good impedance matching is achieved. The tiny difference is caused by the coupling of the EMSAA elements. The 2D radiation patterns at the resonant frequency are depicted in Fig. 8(b). The main-beam patterns are all along the normal direction and the gain reaches 14.4 dBi. The maximum cross-polarization level value is 24.0 dB lower than that of the main-polarization. Electric field distributions are observed on the $8\lambda_{6.76\text{GHz}}$ surface above the EMSAA. As Fig. 8(c) presents, the direction of electric field is along the x-axis direction. Thus, it can be concluded that the EMSAA possesses good radiation properties and radiates x-polarized waves. From the above analysis, it infers that EMSAA also own the ability to radiate y-polarized waves when E2 elements are fed and the feeding phase is 0°.

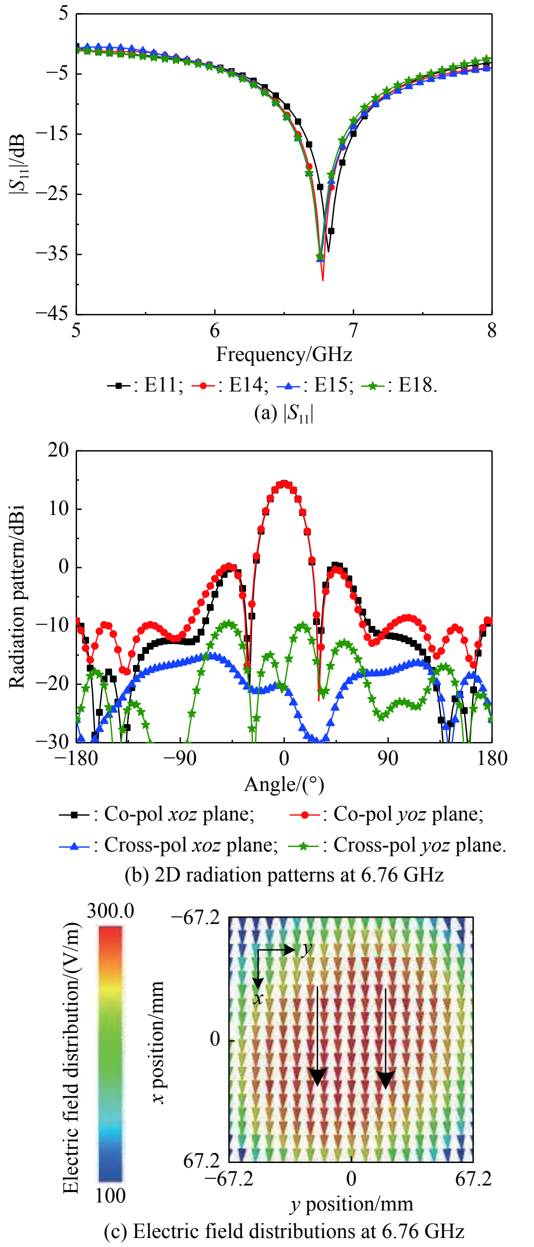

(a) $|S_{11}|$

(b) 2D radiation patterns at 6.76 GHz

(c) Electric field distributions at 6.76 GHz

Fig. 8 ***x*-polarized radiation properties**

Take a further step, the E1 and E2 elements are both fed. The feeding phases of E1 and E2 are 90° and 0°, respectively. The radiation properties of EMSAA in this feeding solution are investigated and shown in Fig. 9.

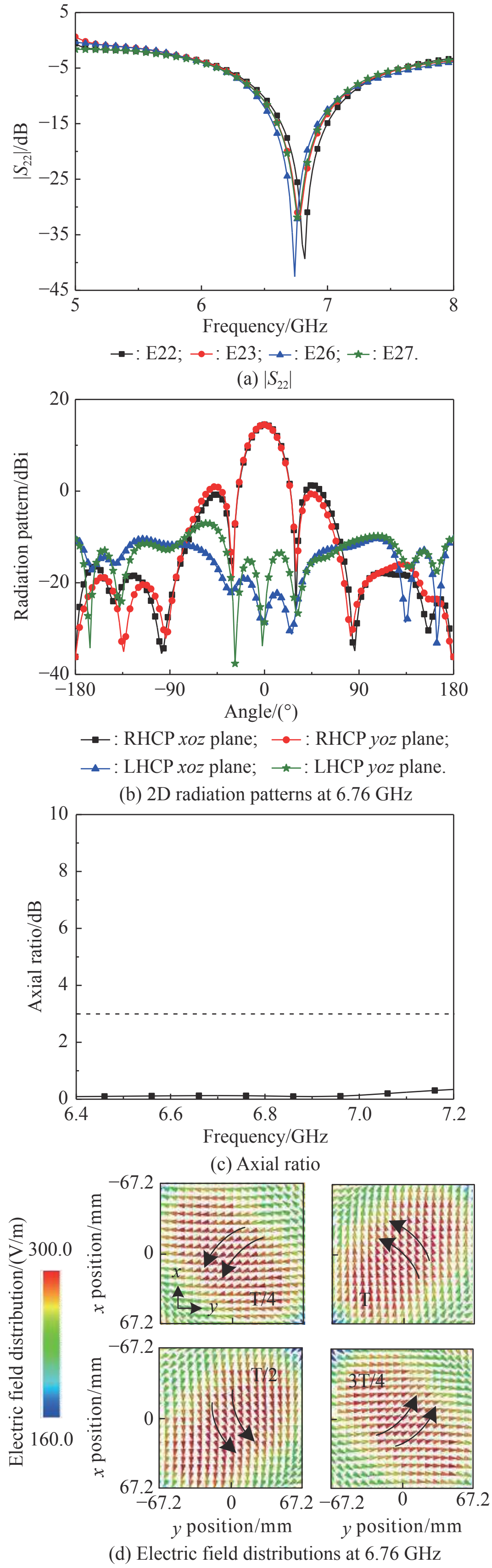

(a) $|S_{22}|$

(b) 2D radiation patterns at 6.76 GHz

(c) Axial ratio

(d) Electric field distributions at 6.76 GHz

Fig. 9 **Right-circular-polarized radiation properties**

To describe the reflection coefficients $|S_{22}|$ of EMSAA, the diagonal elements of EMSAA are selected (E22, E23, E26, E27). As Fig. 9(a) depicts, the elements resonate close to 6.76 GHz and good impedance matching is achieved. The 2D radiation patterns of EMSAA at the resonant frequency are presented in Fig. 9(b). The main-beam patterns are all along the normal direction and the maximum gain is 14.3 dBi. The maximum cross-polarization level value is 20.3 dB lower than that of the main-polarization. The axial ratio of the EMSAA is 0.24 dB in the operation band, shown in Fig. 9(c). Electric field distributions are observed on the $8\lambda_{6.76\text{GHz}}$ surface above the EMSAA at four different moments in a period. As Fig. 9(d) presents, the direction of the electric field rotates anti-clockwise, that is, following the right-hand law. From the above analysis, it can be concluded that the EMSAA possesses good radiation properties and radiates right circular polarized waves. It also can be inferred that EMSAA radiates left circular polarized waves when the E1 and E2 are both fed and feeding phases of E1 and E2 are 0° and 90°, respectively. Moreover, the EMSAA also possesses the potential to radiate elliptical-polarized waves.

Take a further step, the radiation patterns comparison of the EMSAA element and the EMSAA are presented in Fig. 10.

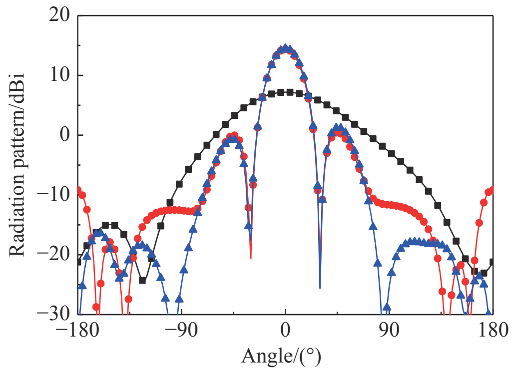

(a) *xoz* plane

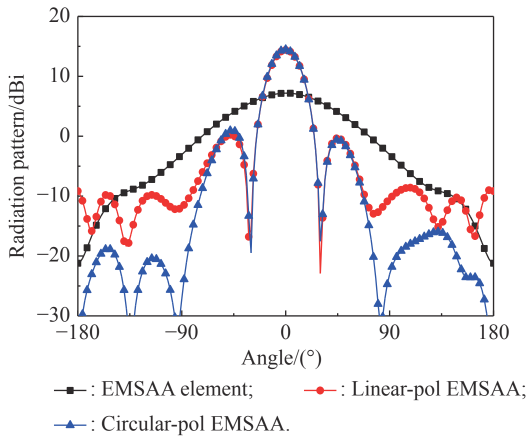

(b) *yoz* plane

Fig. 10 Radiation patterns comparison of EMSAA element and EMSAA

The gains of the linear-polarized EMSAA and circular-polarized EMSAA are almost the same. Compared to the EMSAA element, the gain of EMSAA is enhanced by 7.2 dB. It can be concluded that the EMSAA owns excellent radiation properties to radiate high gain and multi-polarized waves.

4. Fabrication and measurement

To further validate the design method, the proposed EMSAA is fabricated by using the standard printed circuit board (PCB) technology. $|S_{11}|$ is measured by using a vector network analyzer (VNA) Agilent N5230C, and the radiation patterns and the axial ratio are measured in the anechoic chamber.

For the first case, the E1 elements of EMSAA are fed by the 1/8 power divider (RS8W2080-S of REBES) and the same size connecting lines with steady phase and low loss are utilized as phase shifter. Meanwhile, the E2 elements are terminated with matched load, plotted in Fig. 11(a). $|S_{11}|$ of diagonal E1 elements (E11, E14, E15, E18) is measured and shown in Fig. 11(b). The elements resonate close to 7.0 GHz and good impedance matching is achieved. The measured resonant frequency is 0.24 GHz higher than the simulated one, which may be caused by the fabrications. The 2D radiation patterns of EMSAA at the resonant frequency is depicted in Fig. 11(c).

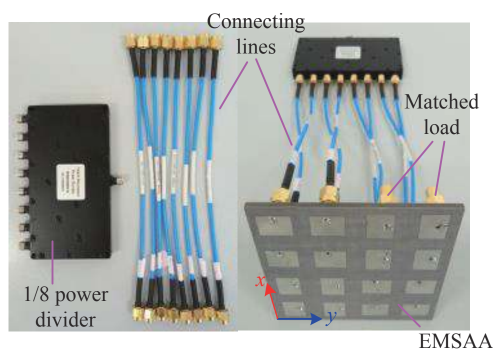

(a) Sample and *x*-polarized measurement configuration

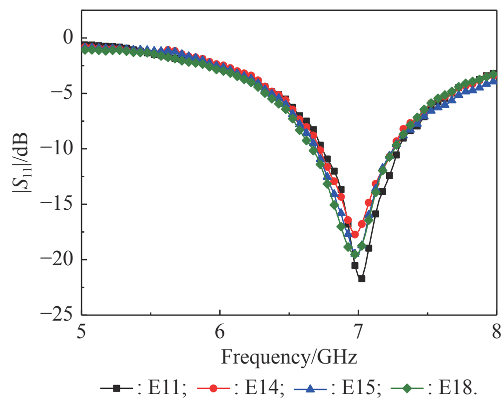

(b) $|S_{11}|$

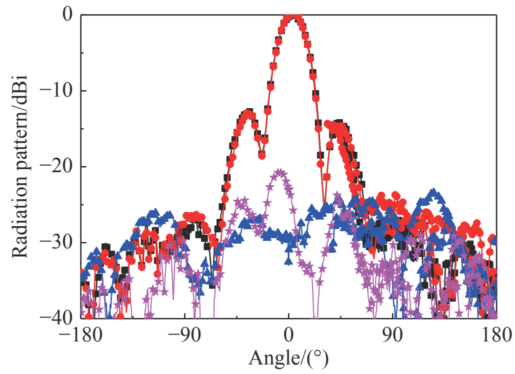

(c) 2D radiation patterns at 7.0 GHz

Fig. 11 *x*-polarized measurement configuration and radiation properties of EMSAA

The main-beam patterns are all along the normal direction and the measured side lobe level values are almost 12.7 dB lower than those of the main lobe level. In addition, the measured results of cross-polarization are all less than −20.6 dB.

For the second case, a 1/2 power divider and two 1/8 power dividers are utilized to feed elements of EMSAA, depicted in Fig. 12(a). To distinguish the feeding phase, two kinds of connecting lines are used. The feeding phase of short connecting lines is 90° ahead of the feeding phase of long connecting lines. As Fig. 12(b) shows, diagonal elements of EMSAA are selected (E22, E23, E26, E27). The elements resonate close to 7.0 GHz and good impedance matching is achieved. The axial ratio of EMSAA is presented in Fig. 12(c), the values of the axial ratio are all less than 3 dB in the operation band while higher than the simulated results. The difference may be caused by bending of connecting lines. As Fig. 12(d) shows, the main-beam patterns are all along normal direction and the measured side lobe level values are 13.9 dB lower than those of the main lobe level. In addition, the measured cross-polarization level values are all less than −19.3 dB.

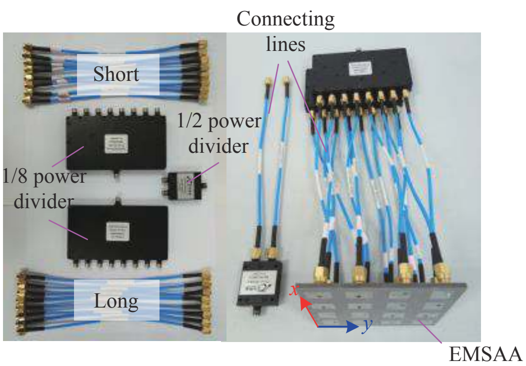

(a) Sample and circular-polarized measurement configuration

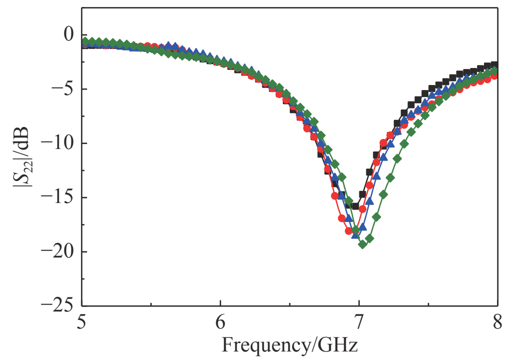

(b) $|S_{22}|$

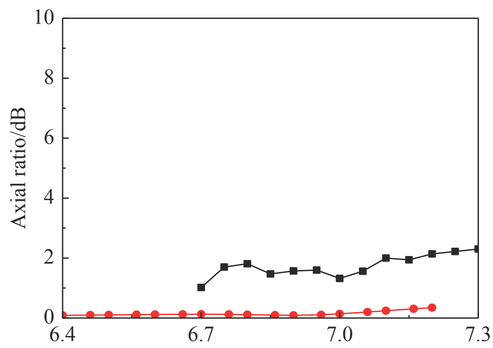

(c) Axial ratio

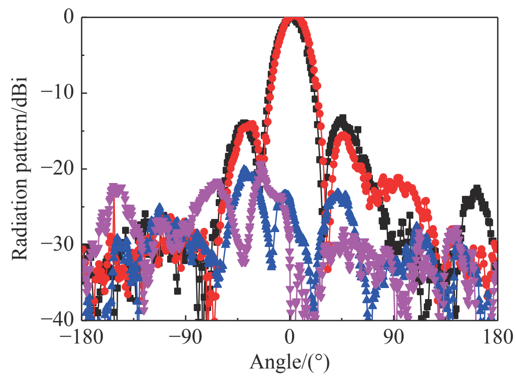

(d) 2D radiation patterns at 7.0 GHz

Fig. 12 Right-circular-polarized measurement configuration and radiation properties of EMSAA

As Fig. 13(a) shows, EMSAA is placed vertically on a foam platform to measure reflection suppression properties. Two horn antennas are initially set as horizontal polarization (*x* polarization in simulation, referring to the coordinate axis). A piece of absorbing material is set between the antennas to reduce undesired coupling. The reflection suppression properties for normal and oblique incident waves are presented in Fig. 13(b). The measured results are consistent with the simulation results. The reflection is suppressed from 5.0 GHz to 8.0 GHz with peak reduction of 14.0 dB, implying 46.2% relative bandwidth. The specular 6 dB reflection suppression is obtained from 5.65 GHz to 7.25 GHz for incident angle below 30°. From the above results, EMSAA possesses good reflection suppression performance. It can be concluded that EMSAA achieves reflection suppression and excellent radiation properties simultaneously.

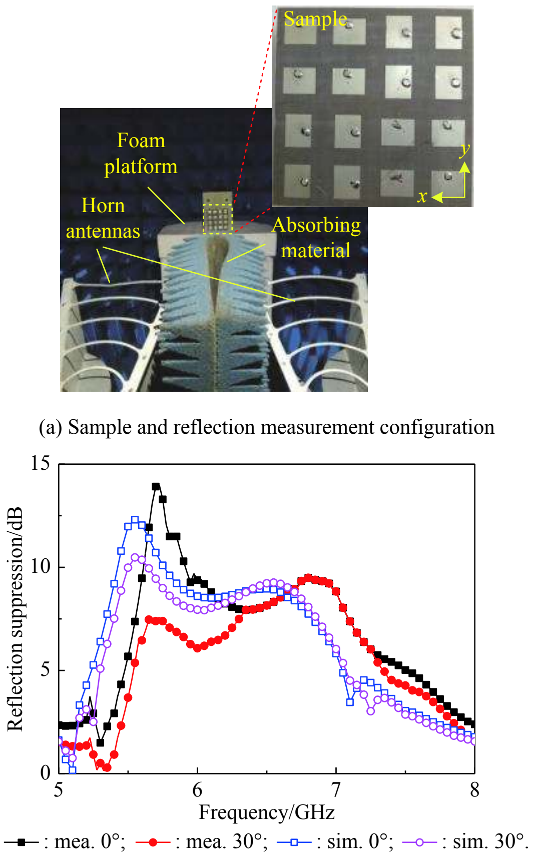

Fig. 13 Reflection measurement configuration and results of EMSAA

Table 1 presents the properties comparison of this paper and the previous articles. For linear polarization, only 8 units of EMSAA work in this paper and [27], while 16 units work in [28] and [30]. For circular polarization, only 16 units of EMSAA work in this paper while 64 units work in [29]. It can be concluded that this work possesses the ability to radiate high gain linear and circular polarization waves. Also, the reflection suppression bandwidth is relatively wide. Same as [27], [28] and [30], the reflection suppression and excellent radiation achieve simultaneously in this paper.

Table 1 Properties comparison of this paper and previous articles

Article	Array size and maximum gain/dBi	Polarized state	Reflection suppression bandwidth/GHz	Working state
[27]	4×4 14	Linear	5.0−8.0	Same time
[28]	4×4 16	Linear	4.0−8.0	Same time
[29]	8×8 17.9	Circular	8.0−13.0	Time sharing
[30]	4×4 17.7	Linear	2.9−3.3	Same time
This paper	4×4 14.3	Linear and circular	5.0−8.0	Same time

5. Conclusions

In this paper, a novel design of EMSAA with reflection suppression and excellent radiation performance is proposed. The element antenna possesses in-phase reflection characteristics and good radiation properties. The EMSAA is formed by using single structured element antenna with 90° rotation and orthometric arrangement. Simulation and experiment results show that linear- and circular-polarized radiation and wideband reflection suppression of EMSAA are achieved simultaneously. It is worth noting that the EMSAA owns the potential to radiate elliptical-polarized waves and this work offers a further strategy to solve the confliction between radiation and scattering of the antenna array.

References

[1] GUO M, SUN Z S, SANG D, et al. Design of frequency-selective rasorbers based on centrosymmetric bended-strip resonator. IEEE Access, 2019, 7: 24964.

[2] CAI T, WANG G M, ZHANG X F, et al. Compact microstrip antenna with enhanced bandwidth by loading magneto-electro-dielectric planar waveguided metamaterials. IEEE Trans. on Antennas and Propagation, 2015, 63(5): 2306–2311.

[3] MA X L, HUANG C, LUO X G, et al. Single layer circular polarizer using metamaterial and its application in antenna. Microwave and Optical Technology Letters, 2012, 54(7): 1770–1774.

[4] JI L Y, GUO Y J, GONG S X, et al. A reconfigurable partially reflective surface (PRS) antenna for beam steering. IEEE Trans. on Antennas and Propagation, 2015, 63(6): 2387–2395.

[5] CHEN Q, SANG D, GUO M, et al. Miniaturized frequency selective rasorber with a wide transmission band using circular spiral resonator. IEEE Trans. on Antennas and Propagation, 2019, 67(2): 1045–1052.

[6] ZHENG Y J, GAO J, CAO X Y, et al. Wideband gain enhancement and RCS reduction of fabry-perot resonator antenna with chessboard arranged metamaterial superstrate. IEEE Trans. on Antennas and Propagation, 2018, 54(2): 590–598.

[7] HONG T, WANG S, GONG S X, et al. RCS reduction and gain enhancement for the circularly polarized array by polarization conversion metasurface coating. IEEE Antennas and Wireless Propagation Letters, 2019, 18(1): 167–171.

[8] SHI Y, MENG Z K, WEI W Y, et al. Characteristic mode

cancellation method and its application for antenna RCS reduction. IEEE Antennas and Wireless Propagation Letters, 2019, 18(9): 1784–1788.
[9] PAQUAY M, IRIARTE J C, EDERRA I, et al. Thin AMC structure for radar cross-section reduction. IEEE Trans. on Antennas and Propagation, 2007, 55(12): 3630–3638.
[10] ZHENG Y J, CAO X Y, GAO J, et al. Shared aperture metasurface with ultra-wideband and wide-angle low-scattering performance. Optical Materials Express, 2017, 7(8): 2706–2714.
[11] YUAN F, XU H X, FU Y Q, et al. RCS reduction based on concave/convex-chessboard random parabolic-phased metasurface. IEEE Trans. on Antennas and Propagation, 2020, 68(3): 2463–2468.
[12] JIA Y T, LIU Y, GONG S X, et al. Broadband polarization rotation reflective surfaces and their applications to RCS reduction. IEEE Trans. on Antennas and Propagation, 2016, 64(1): 179–188.
[13] ORUJI A, PESARAKLOO A, KHALAJ-AMIRHOSSEINI M, et al. Ultrawideband and omnidirectional RCS reduction by using symmetrical coded structures. IEEE Antennas and Wireless Propagation Letters, 2020, 19(7): 1236–1240.
[14] WANG Y, CHEN K, LI Y, et al. Design of non-resonant metasurfaces for broadband RCS reduction. IEEE Antennas and Wireless Propagation Letters, 2021, 20(30): 346–350.
[15] SAMADI F, SEBAK A. Wideband, very low RCS engineered surface with a wide incident angle stability. IEEE Trans. on Antennas and Propagation, 2020. DOI: 10.1109/TAP.2020.3015040.
[16] YANG H H, CAO X Y, YANG F, et al. A programmable metasurface with dynamic polarization, scattering and focusing control. Scientific Reports, 2016, 6: 35692.
[17] LIU S, CUI T J, XU Q, et al. Anisotropic coding metamaterials and their powerful manipulation of differently polarized terahertz waves. Light: Science & Applications, 2016, 5(1): e16076.
[18] ZHENG Y J, GAO J, CAO X Y, et al. Wideband RCS reduction of a microstrip antenna using artificial magnetic conductor structures. IEEE Antennas and Wireless Propagation Letters, 2015, 14: 1582–1585.
[19] LIU Z M, LIU S B, ZHAO X, et al. Wideband gain enhancement and RCS reduction of fabry–perot antenna using hybrid reflection method. IEEE Trans. on Antennas and Propagation, 2020, 68(9): 6497–6505.
[20] JIA Y T, LIU Y, FENG Y J, et al. Low-RCS holographic antenna with enhanced gain based on frequency-selective absorber. IEEE Trans. on Antennas and Propagation, 2020, 68(9): 6516–6525.
[21] LIU Y, LI K, JIA Y T, et al. Wideband RCS reduction of a slot array antenna using polarization conversion metasurfaces. IEEE Trans. on Antennas and Propagation, 2016, 64(1): 326–331.
[22] CHENG Y F, FENG J, LIAO C, et al. Analysis and design of wideband low-RCS wide-scan phased array with AMC ground. IEEE Antennas Wireless and Propagation Letters, 2021, 20(2): 209–213.
[23] PANDIT S, MOHAN A, RAY P. Low-RCS low-profile four-element MIMO antenna using polarization conversion metasurface. IEEE Antennas and Wireless Propagation Letters, 2020, 19(12): 2102–2106.
[24] MENG Z K, SHI Y, WEI W Y, et al. Multifunctional scattering antenna array design for orbital angular momentum vortex wave and RCS reduction. IEEE Access, 2020, 8: 109289–109296.
[25] YIN L, YANG P, GAN Y Y, et al. A low cost, low in-band RCS microstrip phased-array antenna with integrated 2-bit phase shifter. IEEE Trans. on Antennas and Propagation, 2020. DOI:10.1109/TAP.2020.3048575.
[26] ZHENG Q, GUO C J, DING J, et al. A broadband low-RCS metasurface for CP patch antennas. IEEE Trans. on Antennas and Propagation, 2020. DOI: 10.1109/TAP.2020.3030547.
[27] ZHENG Y J, CAO X Y, GAO J, et al. Integrated radiation and scattering performance of a multifunctional electromagnetic surface. Optics Express, 2017, 25(24): 30001–30012.
[28] LIU Y, JIA Y T, ZHANG W B, et al. An integrated radiation and scattering performance design method of low-RCS patch antenna array with different antenna elements. IEEE Trans. on Antennas and Propagation, 2019, 67(9): 6199–6204.
[29] FAN Y, WANG J F, LI Y F, et al. Low-RCS and high-gain circularly polarized metasurface antenna. IEEE Trans. on Antennas and Propagation, 2019, 67(12): 7197–7203.
[30] YANG H H, LI T, XU L M, et al. Low in-band-RCS antennas based on anisotropic metasurface using a novel integration method. IEEE Trans. on Antennas and Propagation, 2020. DOI:10.1109/TAP.2020.3016161.

Biographies

ZHENG Yuejun was born in 1989. He received his B.S., M.S. and Ph.D. degrees from Air Force Engineering University (AFEU), Xi'an, China, in 2012, 2014 and 2018, respectively. In June 2018, he joined the faculty of the National University of Defense Technology (NUDT), Changsha, China, where he is currently a docent. He has authored and coauthored more than 40 scientific papers in major journals and international conferences. His research interests include metamaterial and metasurface, metasurface antenna, radiation and scattering integration technology.
E-mail: zhengyuejun18@nudt.edu.cn

DING Liang was born in 1985. He received his M.E. and Ph.D. degrees in electrical engineering from National University of Defense Technology (NUDT), Changsha, China, in 2010 and 2014, respectively. From 2012 to 2014, he was a visiting researcher in Electromagnetic Imaging Laboratory, University of Manitoba, Winnipeg, Canada. He is currently a lecturer with the College of Electronic Science and Technology, NUDT. His main research interests include inverse problem, metasurfaces and microwave photonics.
E-mail: lio.dingliang@hotmail.com

CHEN Qiang was born in 1991. He received his B.S., M.S. and Ph.D. degrees from National University of Defense Technology (NUDT), Changsha, China, in 2012, 2014 and 2018, respectively, where he is currently a docent. His research interests include artificial electromagnetic materials, electromagnetic materials antenna, circuit analog absorbers, and frequency selective surface.
E-mail: chenqiang08a@nudt.edu.cn

GUO Min was born in 1991. He received his B.S. degree from National University of Defense Technology (NUDT), Changsha, China, in 2016. He is currently working toward his Ph.D. degree in microwave and millimeter wave technology at NUDT, Changsha, China. His research interests include design of frequency selective surface, frequency selective rabsorber, and circuit analog absorbers.
E-mail: guomin14@nudt.edu.cn

FU Yunqi was born in 1975. He received his B.E., M. S. and Ph.D. degrees in 2004, in electronic science and technology from National University of Defense Technology (NUDT), Changsha, China, in 1997, 2000 and 2004, respectively. From 2009 to 2010, he was a visiting scholar at the Ohio State University, America. Since 2011, he has been a professor with NUDT. He has authored or co-authored more than 100 journal papers and three books. His current research interests include artificial electromagnetic metamaterial, microwave and millimeter-wave detection and imaging.
E-mail: yunqifu@nudt.edu.cn